Cantilevers-on-membrane design for broadband MEMS piezoelectric vibration energy harvesting

Yu Jia[1,2], Sijun Du[2] and Ashwin A Seshia[2]

[1]Faculty of Science and Engineering, Thornton Science Park, University of Chester, Chester CH2 4NU, UK

[2]Department of Engineering, University of Cambridge, Trumpington Street, Cambridge CB2 1PZ, UK

E-mail: yu.jia.gb@ieee.org

Abstract. Most MEMS piezoelectric vibration energy harvesters involve either cantilever-based topologies, doubly-clamped beams or membrane structures. While these traditional designs offer simplicity, their frequency response for broadband excitation are typically inadequate. This paper presents a new integrated cantilever-on-membrane design that attempts to both optimise the strain distribution on a piezoelectric membrane resonator and improve the power responsiveness of the harvester for broadband excitation. While a classic membrane-based resonator has the potential to theoretically offer wider operational frequency bandwidth than its cantilever counterpart, the addition of a centred proof mass neutralises its otherwise high strain energy regions. The proposed topology addresses this issue by relocating the proof mass onto subsidiary cantilevers and integrates the merits of both the membrane and the cantilever designs. When experimentally subjected to a band-limited white noise excitation, up to approximately two folds of power enhancement was observed for the new membrane harvester compared to a classic plain membrane device.

1. Introduction

For the last decade, there has been a convergence of vibration energy harvesting (VEH) and microelectromechanical systems (MEMS) technologies [1] in an attempt to eventually realise integrated implementations of VEH and IC platforms for sensor systems. Amongst the different types of miniaturised mechanical-to-electrical transduction mechanisms, electromagnetism does not scale well at dimensions typical of MEMS devices, while electrostatic generators generally demonstrate poor power densities [2]. While there has been a growing trend of adapting electret transducers [3, 4], piezoelectric films remain the most popular choice for MEMS VEH to date [2, 5, 6, 9].

In terms of topologies, cantilever-based designs are by far the most employed structure [2, 5, 6] due to their simplicity, high responsiveness and the ability to house a proof mass near the free end without compromising the high strain energy regions of the active piezoelectric transducer [7, 8]. Membrane designs have been previously investigated in the field [2, 9] and provide the theoretical potential to provide wider frequency bandwidth. However, notable power or bandwidth enhancements from these designs have not been demonstrated yet [10].

One of the main drawbacks of the membrane topology, in comparison to cantilever-based designs, is the strain neutralisation of active piezoelectric transduction regions with the addition

of an effective proof mass. Figures 1 and 2 illustrate a scenario where a significant area of otherwise high strain energy region of a circular disk membrane is sacrificed to house a centred proof mass. Since a given piezoelectric harvester relies on strain-induced charge generation across its active transduction area, strain optimisation is of paramount importance for power optimisation. Furthermore, the additional clamping conditions in a membrane structure yield lower compliance; thus, the membrane requires a higher excitation to manifest the same level of mechanical strain when compared to a cantilever beam.

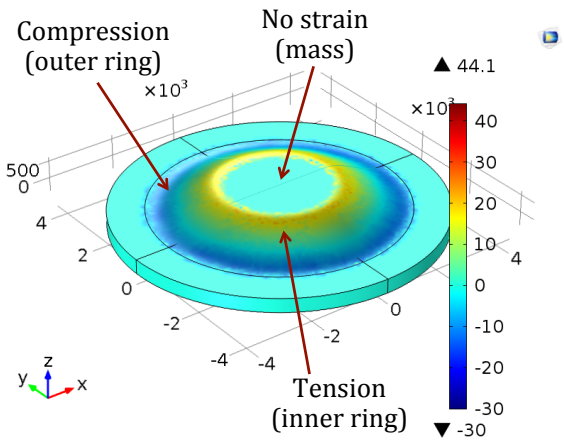

Figure 1: COMSOL model of a classic circular disk membrane (7 mm diameter) and a centred circular suspended proof mass (3 mm diameter).

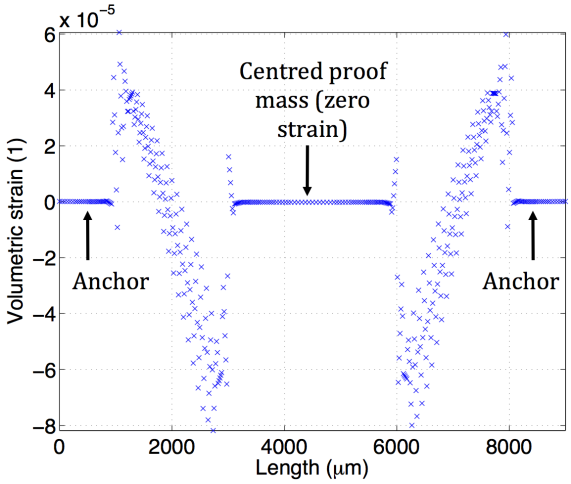

Figure 2: Strain distribution along the diameter of the classic circular disk membrane with an acceleration loading of 100 g.

2. Design and simulation

A new structural topology to improve the responsivity towards broadband excitation is proposed in figure 3. Instead of placing a single proof mass at the membrane centre, the masses are distributed on subsidiary cantilevers that extend outwards from the centre. Although regions of membrane are still sacrificed to accommodate the design complexity, the constant high strain regions of the membrane core are retained (figure 4). Additionally, the subsidiary cantilevers themselves possess high strain regions. Similar to a classic membrane structure, the membrane portion of the new design is composed of two opposing strain regions: the anchor strains near the clamped end and the bending strain near the centre. The bending strain of cantilevers align with that of the membrane core, thereby simplifying electrode design.

Table 2 summarises a simulated and calculated example where the device is subjected to 100 g of acceleration loading on the proof mass. In the simulation, 0.5 μm thick aluminium nitride (AlN) is assumed as the piezoelectric layer. It can be seen that the design complexity of the new membrane topology resulted in smaller total active piezoelectric area. However, as a result of higher compliance of the etched membrane structure as well as the larger effective proof mass, the average induced strain is several folds higher.

The theoretical maximum power extractable from the simulated strain response was calculated by computing the average electric charge generated by equation 1 and the power extractable across an ideal impedance given by equation 2 [8].

$$q = d_{31}\varepsilon_{av}Ea_{pz} \tag{1}$$

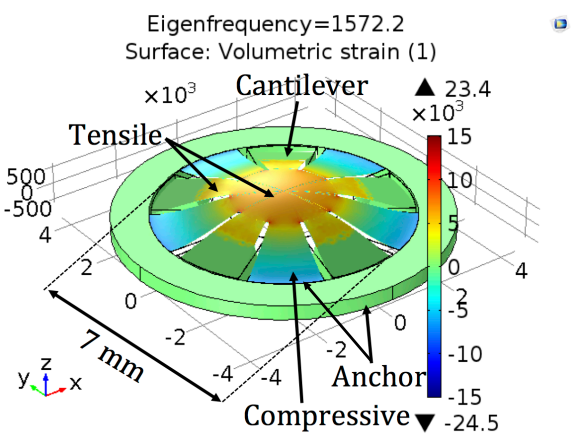

Figure 3: COMSOL model of the integrated cantilever- membrane design with the proof mass distributed on subsidiary cantilevers.

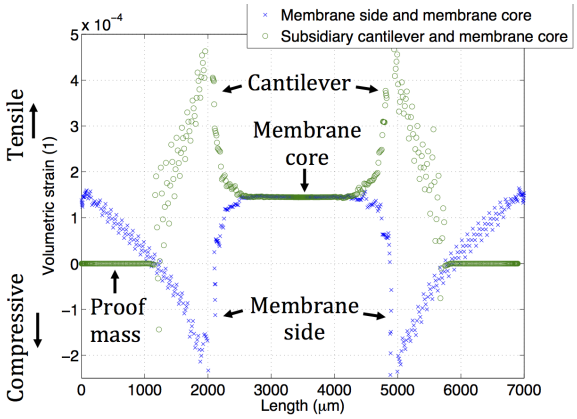

Figure 4: Strain distribution of the integrated cantilever membrane design for 100 g acceleration loading. The centre of the membrane experiences notable strain.

Table 1: Accumulated strain across the active piezoelectric area when subjected to an acceleration loading of 100 g, corresponding to maximum theoretically achievable power amplitude assuming optimal impedance matching for all constituent piezoelectric regions. Av. strain represents average strain across a particular active piezoelectric region.

Parameter	Plain membrane		Cantilever-on-membrane	
	Area (m^2)	av. strain (1)	Area (m^2)	av. strain (1)
Membrane anchor strain	1.88E-5	2.02E-5	7.85E-6	1.03E-4
Membrane bending strain	1.26E-5	4.07E-5	5.23E-6	1.86E-4
Membrane core bending strain	n/a	n/a	7.07E-6	1.29E-04
Cantilever bending strain	n/a	n/a	3.98E-6	2.62E-4
Proof mass (kg)	6.56E-6		8.45E-6	
Natural freq. 01 mode (Hz)	1478		1572	
Sum of area × av. strain (m^2)	8.91E-10		3.73-9	
Charge generated (C)	5.88E-10		2.46E-9	
Theoretical peak power (W)	6.41E-7		1.56E-5	

$$P = \frac{\omega h_p q^2}{\varepsilon_0 \varepsilon_r a_{pz}} \tag{2}$$

where, q is the charge generated, d_{31} is the piezoelectric charge constant in the 31 mode, ε_{av} is the average induced strain, E is the elastic modulus, a_{pz} is the active piezoelectric area, P is the peak power, ω is the frequency, h_p is the thickness of the piezoelectric layer, ε_0 is the permittivity of free space and ε_r is the dielectric constant of the piezoelectric material.

It can be seen from table 2, that given the same design area, the new membrane has the potential to attain a significantly higher peak power. However, this theoretical value is only achievable if all the various active piezoelectric regions are optimally matched in impedance. In practice, due to the complexity of the structure, it is difficult to simultaneously extract maximum energy from both the membrane and the subsidiary cantilevers.

3. Experiment and result

MEMS devices were fabricated using a 0.5 μm AlN on 10 μm doped silicon on insulator process. Un-etched regions of 400 μm thick substrate silicon were used as suspended proof masses. Figure 5 shows a MEMS harvester chip attached to a leadless chip carrier (LCC). The bottom of the LCC was hollowed out, through laser cutting, in order to allow unrestricted travel of the proof masses and minimal film-squeeze damping. Figure 6 presents a closer view of the device. The piezoelectric layer and top metallisation are not integrated on top of the proof masses.

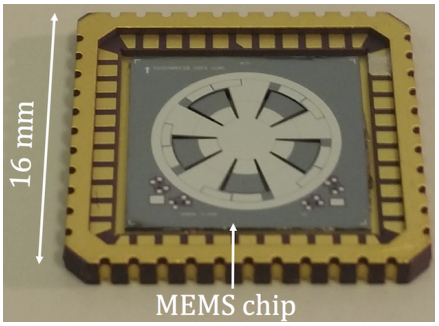

Figure 5: Photograph of the MEMS chip (12 mm by 12 mm) on a leadless chip carrier. The backside of the chip carrier was etched out by laser micro-machining to minimise film-squeeze damping within the package.

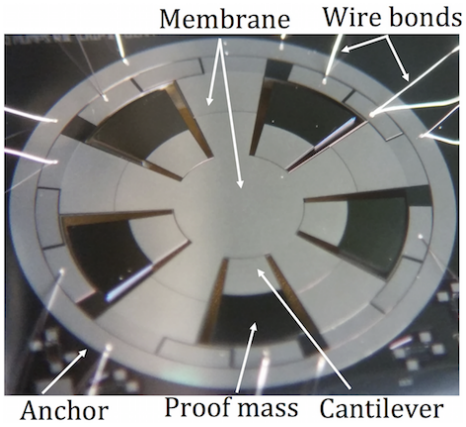

Figure 6: Micrograph of the cantilever-on-membrane VEH (active diameter: 7 mm).

The membrane diameter is 7 mm and the core diameter is 3 mm, while the end mass on each subsidiary cantilever takes up 60% of the cantilever length. While individual electrode zones were segmented during layout design, all transduction regions with the same strain polarity were connected together (off chip) for experimental simplicity. This however, came at the cost of suboptimal impedance matching and power extraction from the harvester. A comparable classic membrane device was also fabricated (7 mm membrane diameter and 3 mm centred mass diameter), which had a less complicated electrode connectivity.

In addition to the 01 mode, the first transverse modes of the subsidiary cantilevers within the new membrane structure can also be employed (table 2) to open up additional operational frequency bands. When driven with 1 g of acceleration at the 01 resonant mode, the plain membrane recorded $\sim$1.2 μW peak power while the new topology device yielded 2.2 μW. The power output of the new topology was 'diluted' by sharing the electrode connection with the cantilevers, which were minimally responsive at the 01 mode frequency range. The subsidiary cantilevers had a much higher compliance than the membrane and produced up to 0.5 μW (each) prior to fracture when driven beyond 0.5 g of acceleration at resonance. On the other hand, the classical membrane was more robust.

Table 2: Frequencies for measured classic membrane and new membrane devices. Modes where strain cancellation takes place are excluded.

Mode of interest	Plain membrane	New membrane
Membrane 01 mode	1200	1400
Subsidiary cantilevers 1 to 5, transverse mode	n/a	280, 290, 300, 310, 320

Figure 7 compares the average power output of the new membrane structure with the classic membrane structure when subjected to band-limited white noise from 10 Hz to 2 kHz. The

experimentally matched load resistance ranged between 50 kΩ to 100 kΩ. However, these values represent a compromise due to the impedance mismatch of the piezoelectric regions on the membrane and the cantilevers.

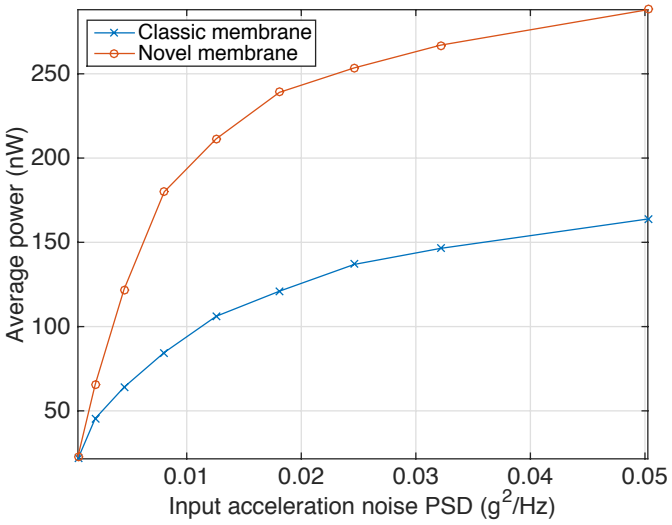

Figure 7: Measured average power for a classic membrane device and a new cantilevers-on-membrane device, subjected to band-limited white noise (10 Hz to 2 kHz).

Up to approximately two folds of power enhancement was observed between 0.005 g^2/Hz and 0.02 g^2/Hz of band-limited white noise. While subsidiary cantilevers readily fractured when driven beyond 0.5 g at resonance, such mechanical failure were not observed when subjected towards the band-limited white noise excitation of up to 0.05 g^2/Hz with peaks at 10 g.

4. Conclusion

A new cantilever-on-membrane topology for MEMS piezoelectric vibration energy harvesting is proposed. Instead of positioning the proof mass at the centre of a classic plain membrane, the masses are distributed onto subsidiary cantilevers. This enabled the harvesting of strain energy at the centre core of the membrane, which would otherwise be neutralised. Furthermore, additional frequency bands were introduced from the subsidiary cantilevers, thus, making it more responsive to broadband excitation. Simulation results suggest the theoretical potential to recover over an order of a magnitude higher peak power for a given acceleration loading, under ideal conditions. Experimentally, the new membrane harvester recorded up to two times higher power output than a plain membrane when subjected to band-limited white noise vibration.

Acknowledgement

This work was supported by the Engineering and Physical Sciences Research Council [EPSRC grant number: EP/L010917/1].

References

[1] A Harb, 2011, Energy harvesting: State-of-the-art, *Renewable Energy*, **36**, 2641-54
[2] S Priya and D Inman, 2009, *Energy Harvesting Technologies*, (New York: Springer US)
[3] F. Peano and T. Tambosso, 205, *J. Microelectromech. Syst.*, **14**(3), 429?35
[4] Y. Suzuki, D. Miki, M. Edamoto, and M. Honzumi, 2010, *J. Micromech. Microeng*, **20**(10)
[5] R. van Schaijk, R. Elfrink, T. Kamel, and M. Goedbloed, 2008, *IEEE Sensors*, 45?48
[6] R Andosca *et al.*, 2012, *Sens. Actuators A.*, **178**, 76-87
[7] Y Jia and A A Seshia, 2014, *J. Phys. Conf. Ser.*, **557**
[8] Y Jia and A A Seshia, 2015, *Microsyst. Technol.*
[9] S. Yoo, J. Kim, S. Park, C. Jang and H. Jeong, 2014, *J. Korean Phys. Soc.*, **64**(5), 706-709
[10] D. Zhu, M.J. Tudor and S.P. Beeby, 2010, *Meas. Sci. Technol.*, **21**(2)